ACS Sustainable Chemistry & Engineering

pubs.acs.org/journal/ascecg

Research Article

Combining Electrocatalysts and Biobased Adsorbents for Sustainable Denitrification

Zili Ma, Matthias Klimpel, Serhiy Budnyk, Anna Rokicińska, Piotr Kuśtrowski, Richard Dronskowski, Aji P. Mathew, Tetyana Budnyak,* and Adam Slabon*

Cite This: *ACS Sustainable Chem. Eng.* 2021, 9, 3658–3667

Read Online

ACCESS | Metrics & More | Article Recommendations | Supporting Information

ABSTRACT: Efficient treatment of domestic and industrial wastewater is one of the major challenges of the 21st century. Among the inorganic pollutants, nitrogen species are significant contaminants and the management of the nitrogen cycle is one the most crucial parts of wastewater purification. Herein, we report an integrated method that minimizes the amount of chemicals used, can be empowered by renewable energy, uses renewables materials for ammonia recovery, and is scalable. Complete denitrification of wastewater was achieved by combining electrochemical and adsorption treatment for real wastewater samples from the Stockholm water pilot plant. About 98% of nitrate was selectively converted to ammonia over abundant copper electrocatalysts in the presence of Na_2SO_4-supporting electrolyte at −0.6 V vs reversible hydrogen electrode (RHE) within 3 h. The valorized nitrate in the form of ammonia could be recovered by means of cheap kraft lignin-SiO_2 sorbents to achieve total denitrification. The presented method is economically feasible, scalable, and contributes to sustainable recycling within a circular economy.

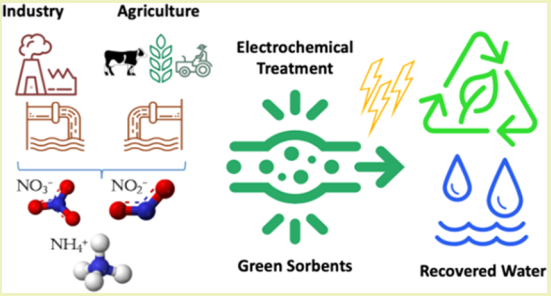

KEYWORDS: *Green chemistry, electrocatalysis, adsorption, nitrate, ammonia production, circular economy, water purification*

INTRODUCTION

The presence of complex types of contamination in domestic and industrial wastewater is considered as one of the major environmental issues.[1,2] Organic and biologic residues, nutrients, pesticides, detergents, metals, and suspended solids are very common pollutants.[3] Traces of medications[4] and drugs are also detected frequently in the wastewater.[5,6] Untreated or improperly treated wastewater can eventually cause diseases and threats to humans and animals. These issues have become critical in many parts of the world and will continue to be important for future wastewater management. The wastewater generated from various, both industrial and domestic, activities has to be purified before reutilization or returning the water back into its natural cycle. Conventional treatment technologies available for wastewater management include physical, chemical, and biological routes.[7] Generally, more than one type of method has to be applied to purify the water depending on the nature of the pollutants.[8]

Among the inorganic pollutants, nitrogen-based compounds such as nitrates and nitrites are a serious concern and need to be addressed. The outflowing water from a water plant is controlled continuously because the purity must meet various guidelines. According to the European legislation, the Nitrate Directive determines that the maximum concentrations of nitrate, nitrite, and ammonium cannot exceed 50, 0.1, and 0.5 $mg \cdot L^{-1}$, respectively.[9] Nowadays, detrimental impacts on the environment have occurred with considerably increasing nitrate concentration in surface and ground waters.[10] High levels of nitrate concentration can overfertilize the soil or change the pH value in the long term or cause eutrophication of water bodies.[11] Nitrate can be also reduced to nitrite in living organisms, which may cause methemoglobinemia, liver damage, or even cancer.[12−14] Hence, the removal of nitrate from water has become a topic of great environmental concern. Although there have been several commercial denitrification technologies developed, such as reverse osmosis, ion exchange, and bacterial denitrification,[15] these solutions are inevitably connected to high costs of post-treatment, harsh operation conditions, and complicated technological processes.

The need for a cost-effective and sustainable denitrification method from discharged effluents has inspired the search for abundant low-cost materials and effective remediation strategies.[16,17] In the past few decades, electrochemical technologies have been explored extensively for addressing environmental problems.[18−20] The biggest advantage within the environmental perspective is the substitution of chemical reagents with the electric current empowered from renewable

Received: October 25, 2020
Revised: February 2, 2021
Published: March 4, 2021

resources.[21] Copper is a prospective electrocatalyst for the reduction of nitrogen-containing compounds because it has a relatively low activity for the hydrogen evolution reaction (HER);[22,23] it also exhibits low toxicity for mammals.[24] This renders copper as the metal of choice for electrochemical reduction of nitrate.[25]

In a circular economy, the desired reduction product of nitrate is ammonia because it could reduce the amount of the latter produced by the energy-consuming Haber–Bosch process.[26] Although the electrochemical reduction of nitrate and nitrite to dinitrogen can be performed by electrocatalysis on simulated wastewater samples that contain no other impurities, real wastewater has a complex composition that makes it easier to control the further reduction process to ammonia. Interestingly, ammonia as an industrial chemical can be easily reclaimed from its aqueous solution via regenerated resins or biobased adsorbent.[27−32] The tailoring of sorbent materials with respect to their surface charge and kinetics offers opportunities for efficient removal of charged compounds from solutions.[33,34] The disadvantage of electrocatalytic nitrate reduction is the applicability of the method to very low concentrations because the required reaction time would meaningfully increase the process costs.

We were interested to develop an efficient and sustainable strategy that minimizes the application of chemicals for the complete removal of nitrate by combining electrocatalysts and sorbent materials (Scheme 1). We demonstrate the application

Scheme 1. Schematic Illustration of the Combined Electrocatalytic and Adsorption Process for Sustainable Nitrate-to-Ammonia Conversion from Wastewater

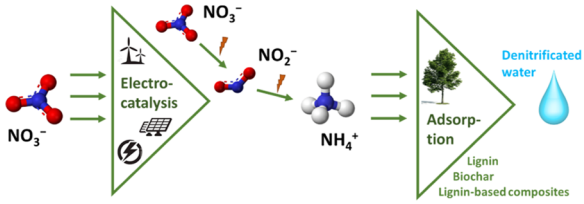

of Cu nanorods (NRs) as electrocatalysts in an environmentally friendly Na_2SO_4 electrolyte and subsequent collection of the final ammonia product by adsorbents. For the post-treatment, several biobased adsorbents including biochar, original kraft lignin, lignosulfonate-, and kraft lignin–silica composites were employed to adsorb the remaining ammonia and traces of nitrate and nitrite.

EXPERIMENTAL SECTION

Preparation of Electrodes. A changed solvothermal method reported by Wang et al.[35] was employed to grow $Cu_2(OH)_3NO_3$ NRs on the Cu substrate. Prior to use, a Cu wire of 0.2 cm in diameter was cleaned for 15 min in an ultrasonic bath of acetone, 1 M diluted HCl (Sigma) solution, and water, respectively. The pristine Cu was added into a 15 mL solution of 2-propanol (>99.7%, Fisher Scientific) solution of 0.12 g copper(II) nitrate trihydrate ($Cu(NO_3)_2{\cdot}3H_2O$, >99%, Sigma) in an autoclave at 433 K for 1 h. After cooling to room temperature, the autoclave was opened and the sample was rinsed with ethanol and water. The dried Cu wire was annealed at 483 K for 4 h under a N_2 atmosphere to yield the CuO NR coating on the bulk Cu wire. Epoxy resin as insulation to define the geometric area for electrochemical experiments. The Cu NRs were obtained by in situ electrochemical CuO NRs in the electrolyte. The fabrication process is summarized in Scheme 2.

Scheme 2. Preparation of Cu NR Electrodes[a]

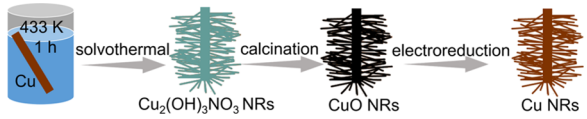

[a]A Cu wire is used as a substrate for the fabrication of CuO NRs via annealing of $Cu_2(OH)_3NO_3$ nanostructures produced by the solvothermal method. Cu NRs are obtained by means of in situ electrochemical reduction of CuO NRs.

Characterization. Powder X-ray diffraction (XRD) patterns were recorded on an STOE STADI-P diffractometer (Cu $K\alpha_1$ radiation) equipped with a DECTRIS Mythen 1K detector in the transmission mode. X-ray photoelectron spectroscopy (XPS) was performed with a Prevac photoelectron spectrometer equipped with a hemispherical analyzer (VG Scienta R3000) and a low-energy flood gun (FS40A-PS). The spectra were recorded using a monochromatized aluminum source Al $K\alpha$ (E = 1486.6 eV). Scanning electron microscopy (SEM) images of the Cu wire were recorded on a Leo Supra 35VP SMT (Zeiss).

Electrochemical Denitrification. The electrochemical experiments were performed in a batch reactor with the conventional three-electrode setup. The working electrode was the Cu NR catalyst, whereas a platinum wire and 1 M Ag/AgCl electrode were used as a counter electrode and a reference electrode, respectively. All potentials were recorded vs 1 M Ag/AgCl and converted vs reversible hydrogen electrode (RHE) according to E_{RHE} (V) = $E_{1MAg/AgCl}$ + (0.059 × pH). A potentiostat (SP-150, BioLogic) operating with the EC Lab Software package and Interface 1010T Workstation (Gamry) was used for all electrochemical experiments. The outflowing wastewater from the Stockholm water plant with or without 0.1 M Na_2SO_4 was used in the electrolyte. Cyclic voltammetry (CV) measurements were performed at a scan rate of 10 mV/s in static solutions. Chronoamperometry (CA) measurements were carried out at given potentials.

Quantitative Analysis. The concentrations of nitrates, nitrites, and ammonia in solutions were determined spectrophotometrically using a Biochrom WPA S800$^+$ Visible Spectrophotometer. In the case of nitrate analysis, the nitration of salicylic acid was considered.[36] The Griess reaction[37] (Merck Spectroquant 114773 and Merck MColortest 114658) was used for the determination of nitrites in solutions. The indophenol method[38,39] (Merck MColortest 114423) and the reaction with the Nessler reagent in the presence of potassium sodium tartrate were used for the quantitative determination of ammonium ions.

Adsorption Denitrification. The post-treatment adsorption of ammonia, as well as trace nitrate and nitrite, was carried out using biochar (Bionaturplus, Germany), kraft lignin (dealkaline, TCI), lignosulfonate-silica (LS-SiO_2), kraft lignin-silica (CF-SiO_2) composites, and the ion-exchange resin Lewatit (Lewatit K-265, Fluka). Biochar, kraft lignin, and Lewatit were used as received without any additional treatment. The LS-SiO_2 composite was synthesized by crosslinking lignosulfonate on the silica gel (0.075–0.250 mm, 15 nm; Acros Organics, Belgium). The CF-SiO_2 composite was synthesized by the sol–gel method via tetraethoxysilane hydrolysis in the activated lignin solution by 3-aminopropyltriethoxysilane. For the synthesis of the composites, lignosulfonic acid sodium salt (LS) (Sigma Aldrich) and membrane-filtered kraft lignin (CF) (CleanFlowBlack, Clean Flow AB, Sweden) were used. The lignin concentrations in LS-SiO_2 and CF-SiO_2 composites were 17 and 680 mg·g^{-1}. The detailed synthetic pathway for LS-SiO_2[34] and CF-SiO_2[40,41] and characterization of composites have been described in our previous works. The adsorption capacity of the applied materials was calculated using the following equation

$$q_{eq} = \frac{(c_0 - c_{eq}) \times V}{m_S} \quad (1)$$

https://dx.doi.org/10.1021/acssuschemeng.0c07807
ACS Sustainable Chem. Eng. 2021, 9, 3658−3667

where q_{eq} is the amount of ions adsorbed per gram of the sorbent ($mg \cdot g^{-1}$) at equilibrium, c_0 and c_{eq} are the initial and equilibrium ion concentrations ($mg \cdot L^{-1}$) in the solution, V is the volume (L) of the initial ion solution, and m_S is the weight of the sorbent (g).

In order to study the effect of phase contact time on the adsorption capacity of sorbents, the following conditions were applied: initial concentration of ammonium ions, 5 $mg \cdot L^{-1}$; volume solutions, 25 mL, and the equilibrium concentrations were measured after 5−90 min. The kinetics of the adsorption process of ammonium ions in various sorbents was investigated using pseudo-first-, pseudo-second-order equations, and the intraparticle diffusion model.

The pseudo-first-order equation is given by[42,43]

$$\log(q_e - q_t) = \log q_e - \frac{kt}{2.303} \quad (2)$$

The pseudo-second-order equation is given as[44,45]

$$\frac{t}{q_t} = \frac{1}{k_2 q_e^2} + \frac{t}{q_e} \quad (3)$$

where q_e and q_t are the amounts of ions adsorbed ($mg \cdot g^{-1}$) at the equilibrium time and at any instant of time t, respectively, K_1 ($1 \cdot min^{-1}$) is the rate constant of the pseudo-first-order adsorption, and K_2 ($g \cdot mg^{-1} \cdot min^{-1}$) is the pseudo-second-order rate constant.

The Weber and Morris equation[46] was applied in order to understand the possibility of intraparticle diffusion

$$q_t = K_{IPD} t^{0.5} + C \quad (4)$$

where K_{IPD} is the intraparticle diffusion rate ($mg \cdot g^{-1} \cdot min^{-0.5}$) and C is a constant.

Adsorption isotherms were obtained by varying the initial ammonium ion concentration between 0.5 and 80 $mg \cdot L^{-1}$. The sorption equilibrium data was applied to the Langmuir, Freundlich, and Temkin models.

The linear form of the Langmuir model is[47]

$$\frac{c_e}{q_e} = \frac{c_e}{q_0} + \frac{1}{K_L q_0} \quad (5)$$

where c_e is the equilibrium concentration of ions ($mg \cdot L^{-1}$), q_e is the amount of the adsorbed ions ($mg \cdot g^{-1}$), and q_0 and K_L are adsorption capacity ($mg \cdot g^{-1}$) and the Langmuir isotherm constant ($L \cdot mg^{-1}$), respectively.

The Freundlich model is[48]

$$\log q_e = \log K_F + \frac{1}{n} \times \log c_e \quad (6)$$

where K_F and n are the Freundlich constants related to the sorption capacity and sorption intensity, respectively.

The Temkin model of isotherm can be expressed as follows

$$c_s = \frac{RT}{b_T} \ln(K_T) + \frac{RT}{b_T} \ln c_{eq} \quad (7)$$

where c_s is the concentration of ions in the solid phase ($mol \cdot g^{-1}$), b_T is the heat of adsorption ($kJ \cdot mol^{-1}$), K_T is the model constant ($L \cdot g^{-1}$), R is the gas constant (8.314 $J \cdot mol^{-1} \cdot K^{-1}$), T represents the absolute temperature (K), and c_{eq} denotes the equilibrium concentration of ions ($mol \cdot L^{-1}$) in the aqueous phase.[49]

RESULTS AND DISCUSSION

Structural Characterization. SEM was first carried out to analyze the morphology of the prepared Cu catalyst. After the solvothermal procedure, several micrometer-level clusters were successfully grown on a Cu wire substrate (Figure S1). The high-magnification image (Figure S1, inset) reveals that the clusters were assembled with uniform NR arrays that were 50−100 nm in diameter and 2−5 μm long. The XRD patterns (Figure S2) indicate that the NRs were of the monoclinic $Cu_2(OH)_3NO_3$ phase (COD No. 1538408). After annealing at 483 K under a N_2 flow, the $Cu_2(OH)_3NO_3$ converted to CuO through a topotactic reaction (SEM of CuO, Figure S3). The conversion to CuO was confirmed by means of powder XRD (Figure S4). Subsequently, the CuO NRs were in situ converted to Cu NRs by electrochemical reduction at a constant negative potential of −0.9 V vs RHE for 10 min. The formation of Cu NRs was confirmed by means of XRD and XPS. The XRD patterns (Figure S4) indicate that the product had the face-centered cubic (fcc) structure of Cu (COD No. 4313207). The reflection peaks at 43.3, 50.8, 74.7, 90.7, and 95.9° correspond to the diffractions of (111), (200), (202), (311), and (222) planes, respectively. Figure 1 presents the

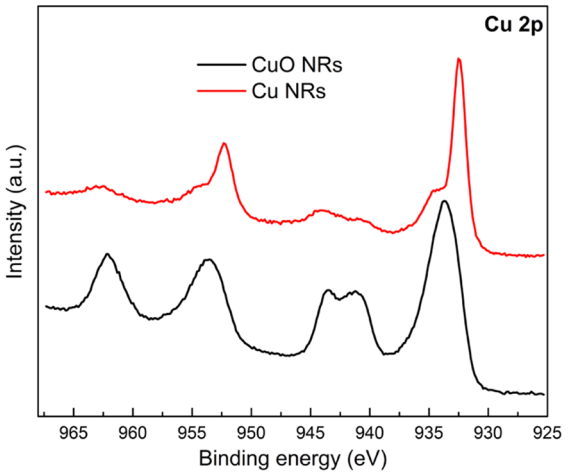

Figure 1. XPS spectra of CuO NRs and Cu NRs.

XPS spectra of CuO NRs and Cu NRs. In the case of the former, it can be confirmed that the Cu $2p_{3/2}$ characteristic peak at 933.7 eV with the satellite peaks corresponds to Cu^{2+}. After the electroreduction step, the characteristic peak shifted to 932.5 eV and became sharper, while the satellite peaks disappeared. This shift clearly confirms the presence of metallic copper in the surface region.

The morphologies of pristine Cu and Cu NRs were compared via SEM. Only several small bulges and shallow pits can be observed on the pristine Cu surface (Figure S5), while the oxide-derived Cu NRs of irregular shape are approximately 50−100 nm in diameter and 2−4 μm long (Figure 2).

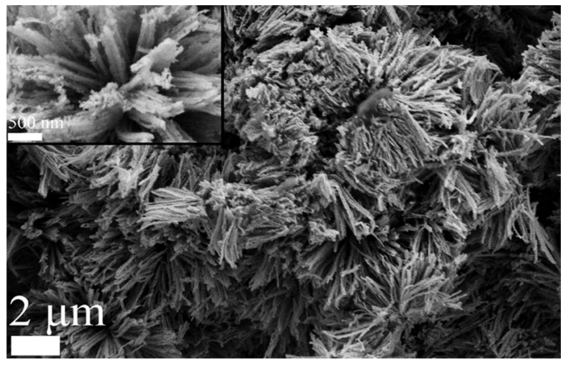

Figure 2. SEM images of Cu NRs. Inset: high-magnification image.

https://dx.doi.org/10.1021/acssuschemeng.0c07807
ACS Sustainable Chem. Eng. 2021, 9, 3658−3667

Electrochemical Denitrification. For the sake of clarity, all concentrations of different ions, i.e., NO_3^-, NO_2^-, and NH_3, are based on the nitrogen mass and given an ending "−N". Excess of Na_2SO_4 was employed as an environmentally friendly electrolyte for electrochemical denitrification of real wastewater samples. This provides a near-neutral environment for the analysis of executable N-containing ions although the pH can change upon production of ammonia. CV was first conducted using the as-prepared Cu NR electrode with a surface area of 9.14 cm^2 in the Na_2SO_4 electrolyte. The first cycle of CV curves exhibits a reduction peak of CuO, which was formed when the electrode was stored in air (Figure 3). In

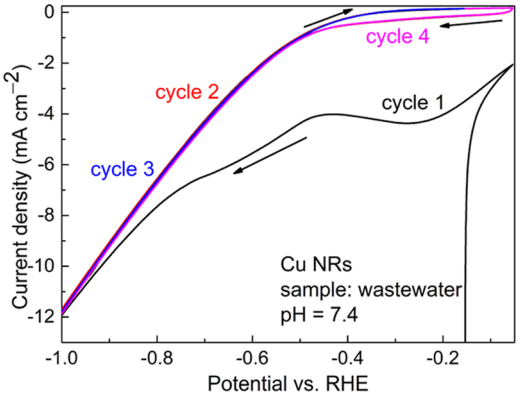

Figure 3. CV curves of Cu NRs with a surface area of 9.14 cm^2 for the wastewater sample in 0.1 M Na_2SO_4 electrolyte at a scan rate of 10 mV/s. The current density relates to the geometric current density.

the second cycle, this cathodic current density disappears in the same potential range. For more cathodic potentials, the current density increases owing to the reduction reactions. Another important phenomenon is that the CV does not show any distinct reduction peaks even up to −1.0 V vs RHE. In the present case, the nitrate and the related intermediate nitrite reduction peaks are overlaid with each other and the competitive HER.

Although the dominant HER occurs at relatively negative potentials, high nitrate and nitrite reduction reactions can be expected. Figure 4 depicts the CA curve recorded at −0.6 V vs RHE with Na_2SO_4-supporting electrolyte. The product concentration after CA for 3 h at −0.6 V vs RHE is

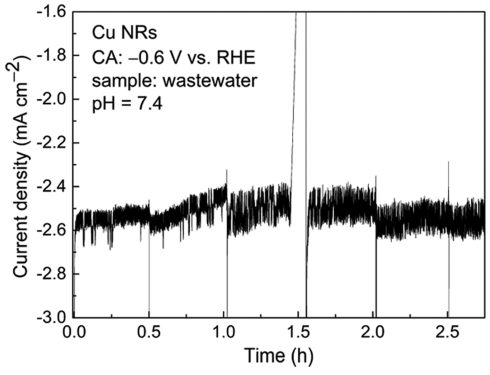

Figure 4. CA of the Cu NRs with a surface area of 9.14 cm^2 in the wastewater sample potential of −0.6 V vs RHE in 0.1 M Na_2SO_4 electrolyte. The interruption at 1.5 h is due to a short contacting problem of the working electrode.

summarized in Figure 5. A significant decrease (98%) of the nitrate was achieved after approximately 2.5 h long CA.

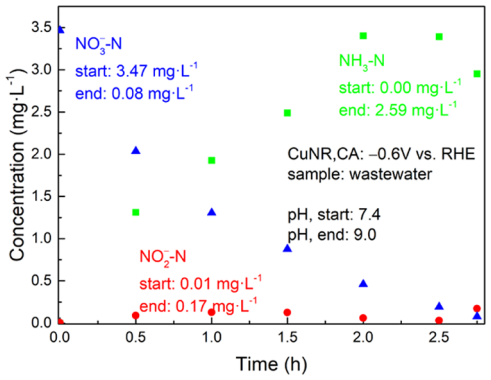

Figure 5. Concentration of nitrate, nitrite, and ammonia vs the electrolysis duration. Electrode surface area A = 9.14 cm^2; applied potential = −0.6 V vs RHE, and 0.1 M Na_2SO_4 supporting electrolyte.

Notably, the ammonia concentration was increased considerably, revealing that the Cu NRs are selective in the nitrate-to-ammonia conversion. The electrolyte had consequently a more basic pH value owing to the formation of ammonia. A similar behavior of the nitrate electroreduction on copper in an alkaline solution (pH 13) has been previously reported by Reyter et al.,[50] where nitrate was only reduced to nitrite at a potential of −0.9 V vs Hg/HgO. When the applied potential shifted to −1.4 V vs Hg/HgO, nitrate-to-ammonia took place. Nitrite was only formed as an intermediate with very low concentrations. This is in agreement with our observation and the change in the concentration decay of nitrate as a function of time indicates a typical first-order reaction.[51]

Although Na_2SO_4 is an environmentally friendly electrolyte and can be recovered by adsorption, it is essential to evaluate the applied electrochemical method with respect to an efficient and economic process for an industrial water purification plant. Within the scope of *Green Chemistry*, the amount of related additives has to be minimized to achieve an efficient atom economy.[52,53]

We, therefore, investigated electrochemical nitrate reduction on Cu NR electrodes for wastewater without the addition of Na_2SO_4 as a supporting electrolyte. It should be noted that experiments were not performed on simulated wastewater samples based on deionized water but on real wastewater samples, which contain a higher conductivity. In the absence of the electrolyte, the developed current density dropped by a factor of 7 (Figure 6) and the CA at −0.6 V vs RHE developed a cathodic current density of 0.45 mA·cm^{-2} (Figure 7). The complementary quantitative analysis showed that the nitrate concentration was only decreased by 39% and the ammonia yield was 1.05 mg·L^{-1} after 3 h (Figure 8). This result indicates that Na_2SO_4 is required as a supporting electrolyte for realistic application. Although one may reduce the nitrate concentration by extending the CA duration, it is inevitably connected to higher energy costs and extremely long electrolysis time. The quantitative analysis in Figure 8 shows that even 14 h was not enough to achieve the nitrate concentration below 1 mg·L^{-1}.

Adsorption Experiment. Although 98% nitrate in wastewater has been reduced in 3 h by means of electroreduction, the ammonia has to be subsequently removed before being discharged. This necessitates an integrated process for

https://dx.doi.org/10.1021/acssuschemeng.0c07807
ACS Sustainable Chem. Eng. 2021, 9, 3658−3667

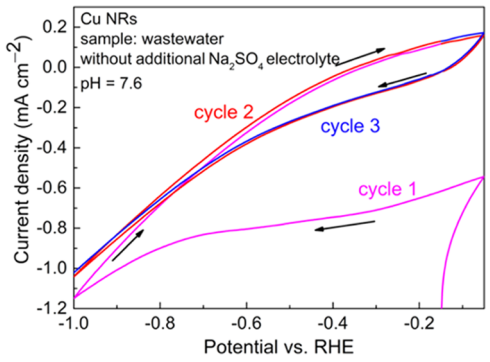

Figure 6. CV of Cu NRs with a surface area of 9.14 cm^2 for the wastewater sample without a supporting electrolyte.

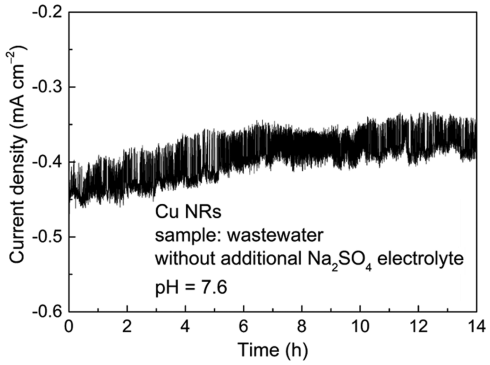

Figure 7. CA of the Cu NRs with a surface area of 9.14 cm^2 for the wastewater sample without a supporting electrolyte. Applied potential = −0.6 V vs RHE.

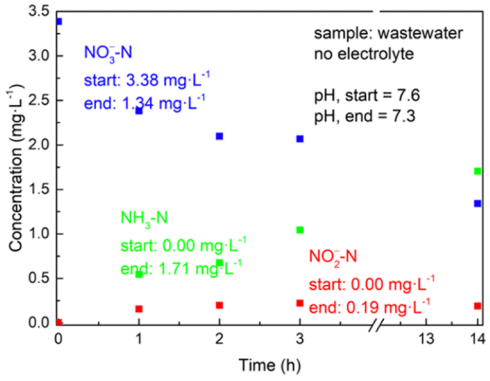

Figure 8. Concentrations of nitrate, nitrite, and ammonia vs the electrolysis duration. Electrode surface area A = 9.14 cm^2; applied potential = −0.6 V vs RHE, and without a supporting electrolyte.

ammonia recovery from the solution to achieve overall circular nitrogen management. Adsorption is an effective method for the removal of variable ions from aqueous solutions. The possibility to run adsorption in near-neutral conditions and to use biomaterials as adsorbents along with preserving the high efficiency of the process renders adsorption as a sustainable method for water purification. A variety of sorbent and membrane materials have been previously studied for ammonium removal.[54−56] Ion-exchange resins were found to be effective because of their good kinetics, capacity, and the possibility to reuse.[57−59] However, nowadays, synthetic ion-exchangers are of concern owing to certain disadvantages associated with their usage, e.g., secondary contamination by organics from the resin, bacterial and chlorine contamination, as well as calcium sulfate and iron fouling. In this regard, there is an urgent need for effective and environmentally friendly sorbents. Lignin is a macromolecule from the wood biomass but still underutilized in comparison to cellulose. Lignin has a unique set of functional groups that can be further chemically modified to yield efficient adsorption. We elucidated therefore lignin and lignin−silica composites based on lignin sulfonate (LS-SiO_2) and kraft lignin (CF-SiO_2) for ammonia removal. We also compared these sorbents with the untreated biochar and with the synthetic cationic ion-exchange resin Lewatit. Since the goal was to develop an integrated system together with electrocatalytic reduction, the adsorption experiments were carried out in the presence of 0.1 M Na_2SO_4 and the most promising systems were compared with the ones without electrolyte.

The determination of pH_{pzc} showed that pure KL and Lewatit are negatively charged in the studied initial pH range from 2 to 12 (pH_{pzc} = 2.0), whereas the biochar and lignin−silica composites are characterized by pH_{pzc} at 6.3, 8.0, and 8.3, respectively (Figure 9a). The study of the influence of the initial concentration of ammonium ions on the adsorption capacity of the studied materials showed that all selected sorbent materials showed adsorption activity toward ammonium ions in the presence of sodium sulfate (Figure 9b). It can be seen from Figure 9b that the lignin-based composites and Lewatit resins are effective in the low range of initial concentrations (≤7.5 mg·L^{-1}) of ammonium ions in the presence of the electrolyte. The adsorption capacities, determined from isotherms, were found to be 4.5 mg·L^{-1} for CF-SiO_2, 4.9 mg·L^{-1} for biochar, 5.5 mg·L^{-1} for KL, 5.3 mg·L^{-1} for LS-SiO_2, and 10.6 mg·L^{-1} for Lewatit (Figure 9b). The comparison of removal efficiency of ammonium ions by all studied materials showed that pure KL and biochar are not efficient for adsorption of low concentrations of ammonium ions from the aqueous solutions. When increasing the initial concentration of ammonium ions, the removal efficiency of original KL and biochar drastically increased to 47−72 and 29−61% for the systems with initial concentrations of ammonium ions ranging from 10 to 20 mg·L^{-1} in the presence of Na_2SO_4.

The characteristic parameters were calculated from the Langmuir, Freundlich, and Temkin isotherm models and are summarized in Table 1. Based on the Langmuir isotherm model, the capacity of the monolayer was found to be 8.99, 4.84, and 5.20 mg·g^{-1} for LS-SiO_2, CF-SiO_2, and KL, respectively. The favorability of the adsorption of ammonium ions was confirmed by the positive R_L values in the range $0 \leq R_L \leq 1$. The calculated K_F was highest for LS-SiO_2 (3.03 mg·g^{-1}) and the Lewatit resin (2.98 mg·g^{-1}). The heat of adsorption of ammonium ions was found to be in the range 0.57−1.326 kJ·mol^{-1} for Lewatit, biochar, and LS-SiO_2 with the highest binding energy (K_T) for biochar (3.638 L·g^{-1}). The highest correlation coefficients (R^2) for all models were found for lignin-based composites (Figure S6).

According to the higher efficiency of lignin-based composites in the range of low concentrations of ammonium ions and their sustainability of initial components, we focused on LS-SiO_2 and CF-SiO_2 composites in our following detailed investigation of the adsorption process.

As a result of the different pulping processes for initial lignins that were used for the synthesis of the composites, LS lignin is characterized by the presence of sulfonic groups in

https://dx.doi.org/10.1021/acssuschemeng.0c07807
ACS Sustainable Chem. Eng. 2021, 9, 3658−3667

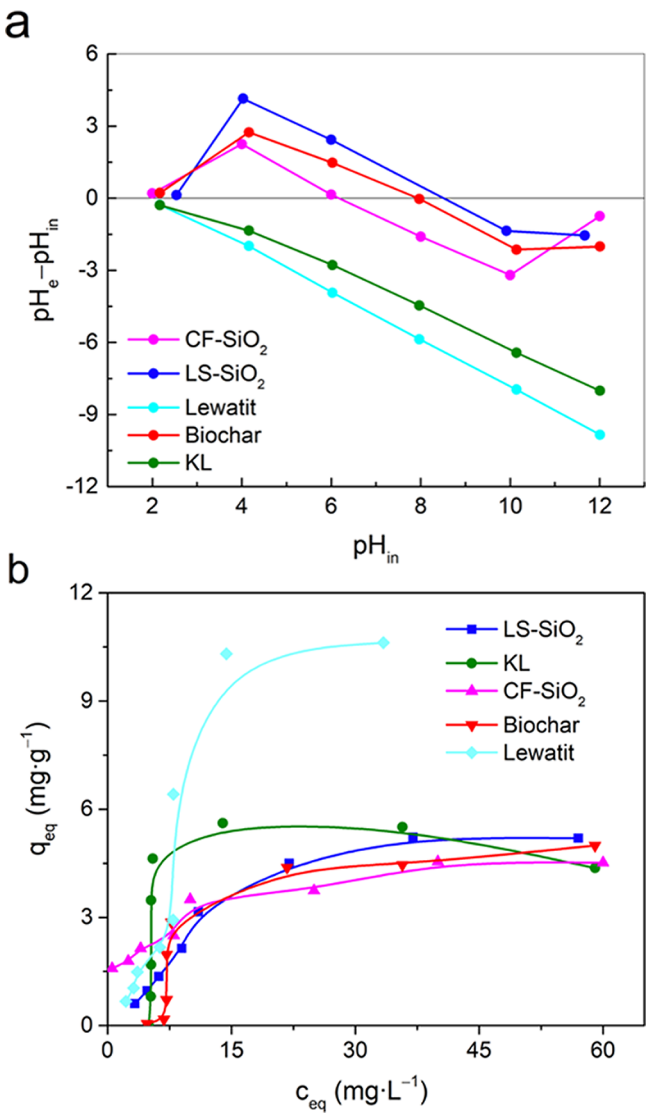

Figure 9. (a) Determination of pH_{pzc} and (b) comparison of adsorption isotherms of ammonium ions by LS-SiO_2, CF-SiO_2, Lewatit resin, biochar, and KL in the presence of electrolyte ions (time of contact: 2 h; initial concentration of ammonium ions: 5−80 mg·L^{-1}; sorbents dosage: 4 g·L^{-1}; shaking rate: 180 rpm; temperature: 22 °C).

addition to the set of hydroxyl and carboxyl groups present in the structure of CF lignin. The selected lignin-based sorbents are characterized by different concentrations of lignin in the composite: 17 mg·g^{-1} for LS-SiO_2 and 680 mg·g^{-1} for CF-SiO_2 according to thermal analysis (Figure S7). Higher content of silica in the LS-SiO_2 composite results in the higher Brunauer−Emmett−Teller (BET) specific surface area (S_{BET}) compared to that in the CF-SiO_2. Thus, the S_{BET} values were 240 m^2·g^{-1} and 92 m^2·g^{-1} for LS-SiO_2 and CF-SiO_2, respectively.[34]

As described earlier by Bernal and Lopez-Real,[60] there are a number of numerous individual processes that could meaningfully influence the ammonium ion adsorption on charged surfaces. These include (i) diffusion of ammonia into or from the atmosphere into the solution; (ii) intraparticle diffusion of ammonia in the gaseous phase; (iii) adsorption of ammonia gas on the solid surface including pores; (iv) equilibrium between the ammonia gas and ammonia in the solution; (v) chemical equilibrium between ammonia and the ammonium ions; and (vi) adsorption of the ammonium equilibrium form to the protonated adsorption sites.

Table 1. Isotherm Model Parameters Obtained for Ammonium Ion Adsorption onto LS-SiO_2, CF-SiO_2, KL, Biochar, and Lewatit at 22 °C in the Presence of 0.1 M Na_2SO_4 Electrolyte[a]

isotherm model/ parameter	LS-SiO_2	CF-SiO_2	KL	biochar	Lewatit
Langmuir					
q_m (mg·g^{-1})	8.99	4.84	5.20	8.40	
K_L (L·mg^{-1})	0.031	0.223	0.174	0.029	
R_L (L·mg^{-1})	0.139	0.082	0.035	0.462	
R^2	0.802	0.989	0.771	0.466	0.001
Freundlich					
K_F (mg·g^{-1})	3.03	1.64	1.10	26.27	2.98
$1/n$	0.771	0.256	0.472	1.357	1.116
R^2	0.893	0.923	0.361	0.539	0.877
Temkin					
b_T (kJ·mol^{-1})	1.326	22.25	1.797	1.234	0.570
K_T (L·g^{-1})	2.527	20.62	1.071	3.638	2.43
R^2	0.959	0.344	0.394	0.822	0.841

[a]Time of contact: 2 h; initial concentration of ammonium ions: 5−80 mg·L^{-1}; sorbents dosage: 4 g·L^{-1}, shaking rate: 180 rpm; and temperature: 22 °C.

In order to understand the mechanism leading to ammonium adsorption and to determine the adsorption rate-controlling step, a kinetic study was conducted.[61] The study of the influence of contact time between phases on the adsorption showed that for LS-SiO_2 the adsorption capacity increased with time and the minimum required time was 15 min. In the case of the CF-SiO_2 composite, the highest extent of removal of ammonium ions was reached after 5 min of contact of the composite with the adsorbate solution at a chosen concentration (Figure S8). The kinetic parameters were obtained from the applied experimental data to the pseudo-first-order, pseudo-second-order equations, and the intraparticle diffusion model; also summarized in Table 2. The kinetic model fitting plots are presented in Figure S9. It was found that the adsorption kinetics for both composites could be well described by the pseudo-second-order equation according to high values of R^2, which were found to be 0.997 and 0.978 for LS-SiO_2 and CF-SiO_2, respectively. The equilibrium sorption capacity ($q_{e,cal}$) and the pseudo-second-order rate constant

Table 2. Kinetic Parameters for the Adsorption of Ammonium Ions on LS-SiO_2 and CF-SiO_2 Composites in the Presence of 0.1 M Na_2SO_4 Electrolyte[a]

kinetics model	parameter symbol (unit)	LS-SiO_2	CF-SiO_2
pseudo-first order	$q_{e,cal}$ (mg·g^{-1})	3.60	1.29
	K_1 (1·min^{-1})	0.007	0.001
	R^2	0.449	0.378
pseudo-second order	$q_{e,cal}$ (mg·g^{-1})	0.27	0.01
	K_2 (g·mg^{-1}·min^{-1})	1.664	12.92
	R^2	0.997	0.978
intraparticle diffusion model	K_{IPD} (mg·g^{-1}·$min^{-0.5}$)	0.03	0.02
	C	0.062	0.184
	R^2	0.567	0.561

[a]Initial concentration of ammonium ions: 5 mg·L^{-1}; sorbents dosage: 8 g·L^{-1}; shaking rate: 180 rpm; and temperature: 22 °C.

https://dx.doi.org/10.1021/acssuschemeng.0c07807
ACS Sustainable Chem. Eng. 2021, 9, 3658−3667

(K_2) were determined from the slope and intercept of the linear relationship t/q_t vs t (Figure S9b). It was found that K_2 is higher for the CF-SiO_2 composite (12.92 g·mg^{-1}·min^{-1}). According to the nonlinear plots q_t vs $t^{0.5}$ (Figure S9b), the chemical reaction controls mainly the rate of adsorption and diffusion to a smaller degree. The obtained results based on the kinetic study are in line with the previously published data concerning the adsorption of ammonium ions; however, the influence of the presence of Na_2SO_4 electrolyte solution in the system results in the competition of the Na^+ ions with the NH_4^+ ions.

Despite the fact that the short time of phase contact was found to be beneficial for the system CF-SiO_2/Na_2SO_4 and longer time for the system LF-SiO_2/Na_2SO_4, it was decided to conduct the equilibrium study for both composites with a short time of contact. This is more convenient for large-scale applications where dynamic sorption is more convenient. The obtained isotherms of adsorption were compared with the ones with a longer-phase contact time (24 h) with or without the presence of an electrolyte. It can be seen from Figure 10 that

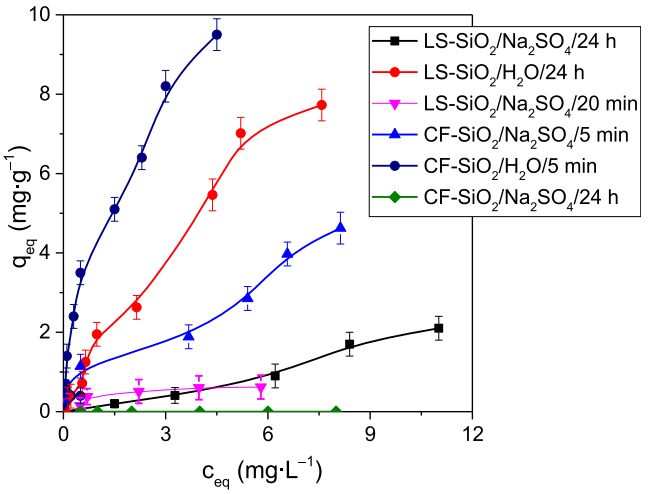

Figure 10. Adsorption isotherms of ammonium ions with 0.1 M Na_2SO_4 or deionized H_2O at 22 °C (initial concentration of ammonium ions: 0.5−25 mg·L^{-1}; sorbent dosage: 4 g·L^{-1}; shaking rate: 180 rpm) with varying contact times.

the capacity of composites is higher for the systems without the addition of an electrolyte: 7.7 mg·g^{-1} for the system LS-SiO_2/H_2O/24 h and 9.5 mg·g^{-1} for CF-SiO_2/H_2O/24 h. With the addition of Na_2SO_4 to the system, the adsorption capacity decreased. This effect could be connected to the change in the ionic strength of the solution and to the competition of Na^+ ions with the NH_4^+ ions for the negatively charged adsorption sites of the composite: −COOH and −OH of the lignin and silica, respectively

During the first 5 min of contact with ammonium ions and in the presence of the electrolyte salt in the system, it is possible to remove 4.6 mg of ammonia by 1 g of the CF-SiO_2 composite. Increasing the time of adsorption leads to sodium ions occupying the adsorption sites of the composite material and the adsorption of ammonium ions decreased. For the systems with LS-SiO_2 in the presence of Na_2SO_4, longer time resulted in a higher capacity of the composite toward ammonium ions (2.1 mg·g^{-1} after 24 h of contact); however, during the 20 min of contact, it is possible to remove 0.62 mg of ammonia by 1 g of the LS-SiO_2 composite.

The Langmuir, Freundlich, and Temkin isotherm models were applied to analyze the obtained data. The characteristic parameters for each isotherm were determined from the fitting plots (Figure S10) and are summarized in Table 3. The

Table 3. Isotherm Model Parameters Obtained for Ammonium Ion Adsorption onto LS-SiO_2 and CF-SiO_2 at 22 °C[a]

	LS-SiO_2			CF-SiO_2	
	Na_2SO_4	Na_2SO_4	H_2O	Na_2SO_4	H_2O
isotherm model/ parameter	(20 min)	(24 h)	(24 h)	(5 min)	(24 h)
Langmuir					
q_m (mg·g^{-1})	0.69	2.01	12.9	5.22	10.36
K_L (L·mg^{-1})	1.610	0.135	0.179	0.341	1.142
R_L (L·mg^{-1})	0.003	0.035	0.034	0.018	0.017
R^2	0.906	0.999	0.547	0.708	0.093
Freundlich					
K_F (mg·g^{-1})	3.23	1.47	1.52	1.24	3.46
$1/n$	0.474	0.267	0.7174	0.54	0.55
R^2	0.772	0.144	0.836	0.828	0.800
Temkin					
b_T (kJ·mol^{-1})	14.393	2.985	2.367	3.124	1.982
K_T (L·g^{-1})	8.089	1.28	21.40	12.45	53.45
R^2	0.897	0.869	0.671	0.811	0.683

[a]Initial concentration of ammonium ions: 0.5−25 mg·L^{-1}; sorbents dosage: 4 g·L^{-1}; and shaking rate: 180 rpm.

experimental data obtained for the systems LS-SiO_2/Na_2SO_4/24 h and LS-SiO_2/Na_2SO_4/20 min could be described well by the monolayer Langmuir adsorption isotherm model (R^2 = 0.906−0.999). The monolayer capacity (q_m) was found to be 0.69 for the system with a short contact time (20 min) and 2.01 mg·g^{-1} for a long contact time (24 h). The favorability of the adsorption was confirmed by the R_L values ranging between 0 and 1. The systems CF-SiO_2/Na_2SO_4/5 min, CF-SiO_2/H_2O/24 h, and LS-SiO_2/H_2O/24 h could be described by the Freundlich isotherm model confirming more complex multilayer adsorption, with a nonuniform distribution of adsorption heat and affinities over the heterogeneous surface ($R^2 \geq 0.8$). K_F was found to be 1.24−3.46 mg·g^{-1}. The heats of adsorption (b_T) of ammonium ions on the studied composites were found to be in a range from 1.982 to 14.393 kJ·mol^{-1}. The binding energy for the interactions between the adsorbents/adsorbates were 1.28−21.40 L·g^{-1} for LS-SiO_2 and 12.45−53.45 L·g^{-1} for CF-SiO_2. However, the R^2 coefficient was found to be low for the Temkin isotherm model (0.671−0.897).

In summary, the conducted adsorption study reveals that the composites based on lignin and silica (LS-SiO_2 and CF-SiO_2) are prospective sorbent materials for ammonium ions removal from low to high concentrations in the presence of an electrolyte with a short contact time, which is a crucial value for dynamic sorption on an industrial scale. The adsorption activity of LS-SiO_2 is comparable to the synthetic resin Lewatit in the range of low initial concentrations of ammonium ions, whereas at low concentrations an adsorption capacity of the CF-SiO_2 material is much higher than for the resin even after the addition of the supportive electrolyte to the system. This allows us to assume that lignin-based sorbents are promising alternatives to synthetic ion-exchangers. The CF-SiO_2

https://dx.doi.org/10.1021/acssuschemeng.0c07807
ACS Sustainable Chem. Eng. 2021, 9, 3658−3667

adsorbent was employed to adsorb the ammonia after electrochemical treatment of real wastewater solutions containing nitrates and nitrites. The adsorption of up to 87% of ammonia was observed (Figure 11).

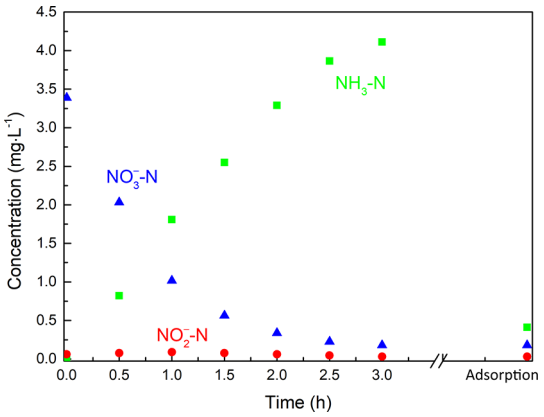

Figure 11. Concentrations of nitrate, nitrite, and ammonia after combined electrocatalysis and adsorption. It should be noted that this graph represents a new experiment with the adsorption step being performed after the end of the CA.

CONCLUSIONS

The electrochemical treatment of nitrate-containing real wastewater has been demonstrated to reduce the concentration below 1 mg·L^{-1} and selectively convert nitrate to ammonia at −0.6 V vs RHE in 3 h with Cu NRs as electrocatalyst in the presence of the Na_2SO_4 electrolyte. During the reduction process, nitrite was only formed as an intermediate at a very low concentration. Control experiments revealed that the supporting electrolyte is essential to reduce nitrate electrochemically. Ammonia could be removed up to 87% from the solution by the CF-SiO_2 adsorbent. However, more experiments are needed to obtain higher profitability such as the optimization of Na_2SO_4 or the NH_3 adsorption procedure, including sorbent recycling. The recycling of the sulfate, which could be realized by a cationic adsorbent, is also an additional possibility. The biobased materials such as cellulose, chitin, and chitosan have already shown promising results with other anions.[62−64]

In conclusion, total denitrification of wastewater has been realized by the combination of electroreduction and adsorption. The materials used in this method are cheap and abundant, and this easily scalable method enables the use of electric current, which can be generated from renewable resources, to reduce the amount of chemicals. This work not only offers us an economic method to realize total denitrification but also provides an exciting new orientation toward the design of practical routes for wastewater treatment with respect to circular nitrogen management.

ASSOCIATED CONTENT

Supporting Information

The Supporting Information is available free of charge at https://pubs.acs.org/doi/10.1021/acssuschemeng.0c07807.

SEM images of $Cu_2(OH)_3NO_3$ NRs; powder XRD patterns of $Cu_2(OH)_3NO_3$; SEM images of CuO NRs; SEM image of pristine Cu; fitting of isotherm and kinetics models, thermal analysis for LS-SiO_2 and CF-SiO_2; influence of phase contact time on the ammonium ion adsorption (PDF)

AUTHOR INFORMATION

Corresponding Authors

Tetyana Budnyak − *Department of Materials and Environmental Chemistry, Stockholm University, 106 91 Stockholm, Sweden; AquaBioSolve Stockholm AB, 186 55 Vallentuna, Sweden;* orcid.org/0000-0003-2112-9308; Email: tetyana.budnyak@mmk.su.se

Adam Slabon − *Department of Materials and Environmental Chemistry, Stockholm University, 106 91 Stockholm, Sweden;* orcid.org/0000-0002-4452-1831; Email: adam.slabon@mmk.su.se

Authors

Zili Ma − *Institute of Inorganic Chemistry, RWTH Aachen University, 52056 Aachen, Germany;* orcid.org/0000-0001-7975-9201

Matthias Klimpel − *Department of Materials and Environmental Chemistry, Stockholm University, 106 91 Stockholm, Sweden*

Serhiy Budnyk − *AC2T research GmbH, 2700 Wiener Neustadt, Austria*

Anna Rokicińska − *Faculty of Chemistry, Jagiellonian University, 30-387 Kraków, Poland;* orcid.org/0000-0001-8397-4422

Piotr Kuśtrowski − *Faculty of Chemistry, Jagiellonian University, 30-387 Kraków, Poland*

Richard Dronskowski − *Institute of Inorganic Chemistry, RWTH Aachen University, 52056 Aachen, Germany; Hoffmann Institute of Advanced Materials, Shenzhen Polytechnic, Shenzhen 518055, China;* orcid.org/0000-0002-1925-9624

Aji P. Mathew − *Department of Materials and Environmental Chemistry, Stockholm University, 106 91 Stockholm, Sweden;* orcid.org/0000-0001-8909-3554

Complete contact information is available at: https://pubs.acs.org/10.1021/acssuschemeng.0c07807

Author Contributions

The manuscript was written through contributions of all authors.

Notes

The authors declare no competing financial interest.

ACKNOWLEDGMENTS

A.S. and A.P.M. thank the Swedish Foundation for Strategic Environmental Research (Mistra: project Mistra SafeChem, project no. 2018/11) for financial support. The authors thank Birgit Hahn for acquiring SEM images. The XPS measurements were carried out with the equipment purchased with the financial support of the European Regional Development Fund in the framework of the Polish Innovation Operational Program (contract no. POIG.02.01.00-12-023/08). Z.M. would like to thank the China Scholarship Council for a Ph.D. scholarship. M.K. acknowledges the financial support from Erasmus+ for his research stay at MMK. The authors also thank IVL for providing us wastewater samples from their pilot plant, and Olena Sevastyanova and Mikael Lindström for providing us the membrane-filtered kraft lignin as a raw material.

https://dx.doi.org/10.1021/acssuschemeng.0c07807
ACS Sustainable Chem. Eng. 2021, 9, 3658−3667

REFERENCES

(1) Nguyen, T. M. H.; Suwan, P.; Koottatep, T.; Beck, S. E. Application of a Novel, Continuous-Feeding Ultraviolet Light Emitting Diode (UV-LED) System to Disinfect Domestic Wastewater for Discharge or Agricultural Reuse. *Water Res.* **2019**, *153*, 53−62.

(2) Köhler, A.; Hellweg, S.; Escher, B. I.; Hungerbühler, K. Organic Pollutant Removal versus Toxicity Reduction in Industrial Wastewater Treatment: The Example of Wastewater from Fluorescent Whitening Agent Production. *Environ. Sci. Technol.* **2006**, *40*, 3395−3401.

(3) Von Sperling, M. *Wastewater Characteristics, Treatment and Disposal*; IWA Publishing, 2007; Vol. *45*.

(4) Kolpin, D. W.; Furlong, E. T.; Meyer, M. T.; Thurman, E. M.; Zaugg, S. D.; Barber, L. B.; Buxton, H. T. Pharmaceuticals, Hormones, and Other Organic Wastewater Contaminants in U.S. Streams, 1999−2000: A National Reconnaissance. *Environ. Sci. Technol.* **2002**, *36*, 1202−1211.

(5) Zuccato, E.; Chiabrando, C.; Castiglioni, S.; Bagnati, R.; Fanelli, R. Estimating Community Drug Abuse by Wastewater Analysis. *Environ. Health Perspect.* **2008**, *116*, 1027−1032.

(6) Irvine, R. J.; Kostakis, C.; Felgate, P. D.; Jaehne, E. J.; Chen, C.; White, J. M. Population Drug Use in Australia: A Wastewater Analysis. *Forensic Sci. Int.* **2011**, *210*, 69−73.

(7) Patwardhan, A. D. *Industrial Waste Water Treatment*; PHI Learing, 2017.

(8) Martínez-Huitle, C. A.; Ferro, S. Electrochemical Oxidation of Organic Pollutants for the Wastewater Treatment: Direct and Indirect Processes. *Chem. Soc. Rev.* **2006**, *35*, 1324−1340.

(9) Martínez, J.; Ortiz, A.; Ortiz, I. State-of-the-Art and Perspectives of the Catalytic and Electrocatalytic Reduction of Aqueous Nitrates. *Appl. Catal., B* **2017**, *207*, 42−59.

(10) Ford, C. L.; Park, Y. J.; Matson, E. M.; Gordon, Z.; Fout, A. R. A Bioinspired Iron Catalyst for Nitrate and Perchlorate Reduction. *Science* **2016**, *354*, 741−743.

(11) Johnston, A. E.; Goulding, K. W. T.; Poulton, P. R. Soil Acidification during More than 100 Years under Permanent Grassland and Woodland at Rothamsted. *Soil Use Manage.* **1986**, *2*, 3−10.

(12) Hill, M. J.; Hawksworth, G.; Tattersall, G. Bacteria, Nitrosamines and Cancer of the Stomach. *Br. J. Cancer* **1973**, *28*, 562−567.

(13) Bartsch, H.; Montesano, R. Relevance of Nitrosamines to Human Cancer. *Carcinogenesis* **1984**, *5*, 1381−1393.

(14) Fewtrell, L. Drinking-Water Nitrate, Methemoglobinemia, and Global Burden of Disease: A Discussion. *Environ. Health Perspect.* **2004**, *112*, 1371−1374.

(15) Duca, M.; Koper, M. T. M. Powering Denitrification: The Perspectives of Electrocatalytic Nitrate Reduction. *Energy Environ. Sci.* **2012**, *5*, 9726.

(16) Ma, Z.; Chen, J.; Luo, D.; Thersleff, T.; Dronskowski, R.; Slabon, A. Structural Evolution of CrN Nanocube Electrocatalysts during Nitrogen Reduction Reaction. *Nanoscale* **2020**, *12*, 19276−19283.

(17) Onwumere, J.; Piątek, J.; Budnyak, T.; Chen, J.; Budnyk, S.; Karim, Z.; Thersleff, T.; Kuśtrowski, P.; Mathew, A. P.; Slabon, A. CelluPhot: Hybrid Cellulose−Bismuth Oxybromide Membrane for Pollutant Removal. *ACS Appl. Mater. Interfaces* **2020**, *12*, 42891−42901.

(18) Dash, B. P.; Chaudhari, S. Electrochemical Denitrificaton of Simulated Ground Water. *Water Res.* **2005**, *39*, 4065−4072.

(19) Chen, G. Electrochemical Technologies in Wastewater Treatment. *Sep. Purif. Technol.* **2004**, *38*, 11−41.

(20) Szewczyk, I.; Rokicińska, A.; Michalik, M.; Chen, J.; Jaworski, A.; Aleksis, R.; Pell, A. J.; Hedin, N.; Slabon, A.; Kuśtrowski, P. Electrochemical Denitrification and Oxidative Dehydrogenation of Ethylbenzene over N-Doped Mesoporous Carbon: Atomic Level Understanding of Catalytic Activity by ^{15}N NMR Spectroscopy. *Chem. Mater.* **2020**, *32*, 7263−7273.

(21) Cid, C. A.; Jasper, J. T.; Hoffmann, M. R. Phosphate Recovery from Human Waste via the Formation of Hydroxyapatite during Electrochemical Wastewater Treatment. *ACS Sustainable Chem. Eng.* **2018**, *6*, 3135−3142.

(22) Worrell, E.; Reuter, M. A. *Handbook of Recycling*; Elsevier, 2014.

(23) van Beers, D.; Kapur, A.; Graedel, T. E. Copper and Zinc Recycling in Australia: Potential Quantities and Policy Options. *J. Cleaner Prod.* **2007**, *15*, 862−877.

(24) Flemming, C. A.; Trevors, J. T. Copper Toxicity and Chemistry in the Environment: A Review. *Water, Air, Soil Pollut.* **1989**, *44*, 143−158.

(25) Reyter, D.; Bélanger, D.; Roué, L. Nitrate Removal by a Paired Electrolysis on Copper and Ti/IrO_2 Coupled Electrodes − Influence of the Anode/Cathode Surface Area Ratio. *Water Res.* **2010**, *44*, 1918−1926.

(26) Rosca, V.; Duca, M.; de Groot, M. T.; Koper, M. T. M. Nitrogen Cycle Electrocatalysis. *Chem. Rev.* **2009**, *109*, 2209−2244.

(27) Ali, I.; Gupta, V. K. Advances in Water Treatment by Adsorption Technology. *Nat. Protoc.* **2006**, *1*, 2661−2667.

(28) Zhang, M.; Zhang, H.; Xu, D.; Han, L.; Niu, D.; Tian, B.; Zhang, J.; Zhang, L.; Wu, W. Removal of Ammonium from Aqueous Solutions Using Zeolite Synthesized from Fly Ash by a Fusion Method. *Desalination* **2011**, *271*, 111−121.

(29) Wang, X.; Lü, S.; Gao, C.; Feng, C.; Xu, X.; Bai, X.; Gao, N.; Yang, J.; Liu, M.; Wu, L. Recovery of Ammonium and Phosphate from Wastewater by Wheat Straw-Based Amphoteric Adsorbent and Reusing as a Multifunctional Slow-Release Compound Fertilizer. *ACS Sustainable Chem. Eng.* **2016**, *4*, 2068−2079.

(30) Budnyak, T. M.; Slabon, A.; Sipponen, M. H. Lignin−Inorganic Interfaces: Chemistry and Applications from Adsorbents to Catalysts and Energy Storage Materials. *ChemSusChem* **2020**, *13*, 4344−4355.

(31) Ray, H.; Perreault, F.; Boyer, T. H. Ammonia Recovery from Hydrolyzed Human Urine by Forward Osmosis with Acidified Draw Solution. *Environ. Sci. Technol.* **2020**, *54*, 11556−11565.

(32) Jantarakasem, C.; Kasuga, I.; Kurisu, F.; Furumai, H. Temperature-Dependent Ammonium Removal Capacity of Biological Activated Carbon Used in a Full-Scale Drinking Water Treatment Plant. *Environ. Sci. Technol.* **2020**, *54*, 13257−13263.

(33) Piątek, J.; de Bruin-Dickason, C. N.; Jaworski, A.; Chen, J.; Budnyak, T.; Slabon, A. Glycine-Functionalized Silica as Sorbent for Cobalt(II) and Nickel(II) Recovery. *Appl. Surf. Sci.* **2020**, *530*, No. 147299.

(34) Budnyak, T. M.; Modersitzki, S.; Pylypchuk, I. V.; Piątek, J.; Jaworski, A.; Sevastyanova, O.; Lindström, M. E.; Slabon, A. Tailored Hydrophobic/Hydrophilic Lignin Coatings on Mesoporous Silica for Sustainable Cobalt(II) Recycling. *ACS Sustainable Chem. Eng.* **2020**, *8*, 16262−16273.

(35) Wang, Z.; Su, F.; Madhavi, S.; Lou, X. W. CuO Nanostructures Supported on Cu Substrate as Integrated Electrodes for Highly Reversible Lithium Storage. *Nanoscale* **2011**, *3*, 1618−1623.

(36) Robarge, W. P.; Edwards, A.; Johnson, B. Water and Waste Water Analysis for Nitrate via Nitration of Salicylic Acid. *Commun. Soil Sci. Plant Anal.* **1983**, *14*, 1207−1215.

(37) Miranda, K. M.; Espey, M. G.; Wink, D. A. A Rapid, Simple Spectrophotometric Method for Simultaneous Detection of Nitrate and Nitrite. *Nitric Oxide* **2001**, *5*, 62−71.

(38) Verdouw, H.; Van Echteld, C. J. A.; Dekkers, E. M. J. Ammonia Determination Based on Indophenol Formation with Sodium Salicylate. *Water Res.* **1978**, *12*, 399−402.

(39) Hoffmann, I.; Nagy, B.; Schneider, J. Methode Zur Bestimmung Des Ammoniakstickstoffes in Gewässern. *Acta Hydrochim. Hydrobiol.* **1984**, *12*, 645−651.

(40) Budnyak, T. M.; Aminzadeh, S.; Pylypchuk, I. V.; Riazanova, A. V.; Tertykh, V. A.; Lindström, M. E.; Sevastyanova, O. Peculiarities of Synthesis and Properties of Lignin−Silica Nanocomposites Prepared by Sol-Gel Method. *Nanomaterials* **2018**, *8*, 950−967.

(41) Budnyak, T. M.; Piątek, J.; Pylypchuk, I. V.; Klimpel, M.; Sevastyanova, O.; Lindström, M. E.; Gun'ko, V. M.; Slabon, A. Membrane-Filtered Kraft Lignin−Silica Hybrids as Bio-Based Sorbents for Cobalt(II) Ion Recycling. *ACS Omega* **2020**, *5*, 10847−10856.

https://dx.doi.org/10.1021/acssuschemeng.0c07807
ACS Sustainable Chem. Eng. 2021, 9, 3658−3667

(42) Derylo-Marczewska, A.; Miroslaw, K.; Marczewski, A. W.; Sternik, D. Studies of Adsorption Equilibria and Kinetics of O-, m-, p-Nitro- and Chlorophenols on Microporous Carbons from Aqueous Solutions. *Adsorption* **2010**, *16*, 359−375.
(43) Marczewski, A. W. Application of Mixed Order Rate Equations to Adsorption of Methylene Blue on Mesoporous Carbons. *Appl. Surf. Sci.* **2010**, *256*, 5145−5152.
(44) Simonin, J. P. On the Comparison of Pseudo-First Order and Pseudo-Second Order Rate Laws in the Modeling of Adsorption Kinetics. *Chem. Eng. J.* **2016**, *300*, 254−263.
(45) Ho, Y. S.; McKay, G. Pseudo-Second Order Model for Sorption Processes. *Process Biochem.* **1999**, *34*, 451−465.
(46) Lagergren, S. Zur Theorie der Sogenannten Adsorption Gelöster Stoffe. *K. Sven. Vetenskapsakad. Handl.* **1898**, *24*, 1−39.
(47) Langmuir, I. The Constitution and Fundamental Properties of Solids and Liquids. Part I. Solids. *J. Am. Chem. Soc.* **1916**, *38*, 2221−2295.
(48) Freundlich, H. Über Die Adsorption in Lösungen. *Z. Phys. Chem.* **1906**, *57U*, 385−490.
(49) Foo, K. Y.; Hameed, B. H. Insights into the Modeling of Adsorption Isotherm Systems. *Chem. Eng. J.* **2010**, *156*, 2−10.
(50) Reyter, D.; Bélanger, D.; Roué, L. Study of the Electroreduction of Nitrate on Copper in Alkaline Solution. *Electrochim. Acta* **2008**, *53*, 5977−5984.
(51) Atkins, P.; de Paula, J. *Atkins' Physical Chemistry*; Oxford University Press, 2018.
(52) Anastas, P.; Eghbali, N. Green Chemistry: Principles and Practice. *Chem. Soc. Rev.* **2010**, *39*, 301−312.
(53) Zimmerman, J. B.; Anastas, P. T.; Erythropel, H. C.; Leitner, W. Designing for a Green Chemistry Future. *Science* **2020**, *367*, 397−400.
(54) Alshameri, A.; He, H.; Zhu, J.; Xi, Y.; Zhu, R.; Ma, L.; Tao, Q. Adsorption of Ammonium by Different Natural Clay Minerals: Characterization, Kinetics and Adsorption Isotherms. *Appl. Clay Sci.* **2018**, *159*, 83−93.
(55) Hu, X.; Zhang, X.; Ngo, H. H.; Guo, W.; Wen, H.; Li, C.; Zhang, Y.; Ma, C. Comparison Study on the Ammonium Adsorption of the Biochars Derived from Different Kinds of Fruit Peel. *Sci. Total Environ.* **2020**, *707*, No. 135544.
(56) Vaičiukynienė, D.; Mikelionienė, A.; Baltušnikas, A.; Kantautas, A.; Radzevičius, A. Removal of Ammonium Ion from Aqueous Solutions by Using Unmodified and H_2O_2-Modified Zeolitic Waste. *Sci. Rep.* **2020**, *10*, No. 352.
(57) Al-Sheikh, F.; Moralejo, C.; Pritzker, M.; Anderson, W. A.; Elkamel, A. Ammonia Removal from Real Wastewater Using a LEWATIT S 108 H Resin: A Batch Process and Fixed-Bed Column. *Sep. Sci. Technol.* **2020**, *55*, 2869−2878.
(58) Wołowicz, A.; Hubicki, Z. The Use of the Chelating Resin of a New Generation Lewatit MonoPlus TP-220 with the Bis-Picolylamine Functional Groups in the Removal of Selected Metal Ions from Acidic Solutions. *Chem. Eng. J.* **2012**, *197*, 493−508.
(59) Al-Sheikh, F.; Moralejo, C.; Pritzker, M.; Anderson, W. A.; Elkamel, A. Batch Adsorption Study of Ammonia Removal from Synthetic/Real Wastewater Using Ion Exchange Resins and Zeolites. *Sep. Sci. Technol.* **2021**, *56*, 462−473.
(60) Bernal, M. P.; Lopez-Real, J. M. Natural Zeolites and Sepiolite as Ammonium and Ammonia Adsorbent Materials. *Bioresour. Technol.* **1993**, *43*, 27−33.
(61) Yi, X.; Xu, Z.; Liu, Y.; Guo, X.; Ou, M.; Xu, X. Highly Efficient Removal of Uranium(VI) from Wastewater by Polyacrylic Acid Hydrogels. *RSC Adv.* **2017**, *7*, 6278−6287.
(62) Zghida, H.; Baouab, M. H. V.; Gauthier, R. Sorption of Chromium Oxy-Anions onto Cationized Ligno-Cellulosic Material. *J. Appl. Polym. Sci.* **2003**, *87*, 1660−1665.
(63) Chassary, P.; Vincent, T.; Guibal, E. Metal Anion Sorption on Chitosan and Derivative Materials: A Strategy for Polymer Modification and Optimum Use. *React. Funct. Polym.* **2004**, *60*, 137−149.
(64) Sundaram, C. S.; Viswanathan, N.; Meenakshi, S. Fluoride Sorption by Nano-Hydroxyapatite/Chitin Composite. *J. Hazard. Mater.* **2009**, *172*, 147−151.

https://dx.doi.org/10.1021/acssuschemeng.0c07807
ACS Sustainable Chem. Eng. 2021, 9, 3658−3667